Crystal Structures of Two Complexes of the Rare-Earth−DOTA−Binding Antibody 2D12.5: Ligand Generality from a Chiral System

ARTICLE *in* JOURNAL OF THE AMERICAN CHEMICAL SOCIETY · JANUARY 2004

Impact Factor: 12.11 · DOI: 10.1021/ja037236y · Source: PubMed

3 AUTHORS, INCLUDING:

Todd Corneillie
Biophor Diagnostics
13 PUBLICATIONS **363** CITATIONS
SEE PROFILE

Andrew Fisher
University of California, Davis
77 PUBLICATIONS **2,540** CITATIONS
SEE PROFILE

J|A|C|S
ARTICLES
Published on Web 11/12/2003

Crystal Structures of Two Complexes of the Rare-Earth-DOTA-Binding Antibody 2D12.5: Ligand Generality from a Chiral System

Todd M. Corneillie, Andrew J. Fisher, and Claude F. Meares*

Contribution from the Department of Chemistry, University of California, One Shields Avenue, Davis, California 95616

Received July 11, 2003; E-mail: cfmeares@ucdavis.edu

Abstract: We report the crystal structures of antibody 2D12.5 Fab bound to an yttrium-DOTA analogue and separately to a gadolinium-DOTA analogue. The rare earth elements have many useful properties as probes, and 2D12.5 binds the DOTA (1,4,7,10-tetraazacyclododecane-*N*,*N*′,*N*″,*N*‴-tetraacetic acid) complexes of *all* of them (Corneillie et al. *J. Am. Chem. Soc.* **2003**, *125*, 3436−3437). The structures show that there are no direct protein−metal interactions: a bridging water acts as a link between the protein and metal, with the chelate present as the **M** isomer in each case. DOTA forms an amphipathic cylinder with the charged carboxylate groups toward the face of the chelate near the metal ion, while nonpolar methylene groups from the macrocycle and the carboxymethyl groups occupy the rear and sides of the molecule. The orientation of the metal-DOTA in the 2D12.5 complex places most of the methylene carbon atoms of DOTA in hydrophobic contact with aromatic protein side chains. Other binding interactions between the metal complex and the antibody include a bidentate salt bridge, four direct H-bonds, and four to five water-mediated H-bonds. We find that 2D12.5 exhibits enantiomeric binding generality, binding yttrium chelates in both $\Lambda(\delta\delta\delta\delta)$ and $\Delta(\lambda\lambda\lambda\lambda)$ configurations with modestly different affinities. This develops from the symmetrical nature of the DOTA chelate, which places heteroatoms and hydrophobic atoms in approximately the same relative positions regardless of the helicity of DOTA.

Introduction

The discovery of molecular pairs exhibiting strong, specific binding interactions and their development into tools for biological, medical, and other applications play an important role in many areas of chemistry. An example is the unusually stable complex between the protein avidin and the small organic molecule biotin, which not only is specific but also can be practically irreversible over the course of several hours in aqueous solution. The avidin−biotin pair or the similar streptavidin−biotin pair provides the basis for applications ranging from specific stains and assays in the laboratory to targeted radiotherapy of cancer.[1−4]

Another class of binding interactions is represented by antibody−antigen complexes, which can involve a wide variety of antigens, both natural and synthetic. Antibody 2D12.5 was originally developed to trap yttrium-DOTA[5] chelates in tumors for cancer therapy.[6−8] The original antigen for the monoclonal antibody 2D12.5 was the stereochemically pure DOTA derivative (*S*)BAD complexed to Y^{3+}, conjugated to the immunogenic protein KLH via a 2IT linker.[8] DOTA forms unusually stable complexes with a wide variety of metal ions including the trivalent rare earths.[9−11] Metal complexes of DOTA and numerous synthetic DOTA derivatives have been developed for a variety of purposes, generally involving the use of the metal ions as probes.[12−14] Side chains act as molecular handles for

(1) Gygi, S. P.; Rist, B.; Gerber, S. A.; Turecek, F.; Gelb, M. H.; Aebersold, R. *Nat. Biotechnol.* **1999**, *17*, 994−999.
(2) Ranish, J. A.; Yi, E. C.; Leslie, D. M.; Purvine, S. O.; Goodlett, D. R.; Eng, J.; Aebersold, R. *Nat. Genet.* **2003**, *33*, 349−355.
(3) Zhang, M.; Zhang, Z.; Garmestani, K.; Schultz, J.; Axworthy, D. B.; Goldman, C. K.; Brechbiel, M. W.; Carrasquillo, J. A.; Waldmann, T. A. *Proc. Natl. Acad. Sci. U.S.A.* **2003**, *100*, 1891−1895.
(4) Pagel, J. M.; Hedin, N.; Subbiah, K.; Meyer, D.; Mallet, R.; Axworthy, D.; Theodore, L. J.; Wilbur, D. S.; Matthews, D. C.; Press, O. W. *Blood* **2003**, *101*, 2340−2348.

(5) Abbreviations: 2IT, 2-iminothiolane; CAPS (3-(cyclohexylamino)-1-propanesulfonic acid) buffer, 10 mM CAPS, 100 mM NaCl, pH 10; CDR, complementarity determining region; DOTA, 1,4,7,10-tetraazacyclododecane-*N*,*N*′,*N*″,*N*‴-tetraacetic acid; DTPA, diethylenetriamine-*N*,*N*,*N*′,*N*″,*N*″-pentaacetic acid; Endo F2, Endo-*β*-*N*-acetylglucosaminidase F2; Fab, antigen-binding fragment of an antibody (V_H and V_L, variable domains of an antibody heavy chain and light chain, respectively; C_{H1} and C_L, constant domains of the light and heavy chain comprising the constant domain part of the Fab); Ga-HBED, gallium-*N*,*N*′-di(2-hydroxybenzyl)ethylenediamine-*N*,*N*′-diacetic acid; ELISA, enzyme-linked immunosorbent assay; KLH, keyhole limpet hemocyanin; mAb, monoclonal antibody; MWCO, molecular weight cutoff; NMWL, nominal molecular weight limit; rmsd, root-mean-square deviation; (*S*)BAD, ((*S*)-2-(4-(2-bromo-acetamido)-benzyl)-DOTA); (*S*)HETD, ((*S*)-2-(4-(2-(2-hydroxyethylthio)-acetamido)-benzyl)-DOTA); (*S*)EOTUBE, (*S*)-2-(4-(3-(2-hydroxyethyl)-thioureido)-benzyl)-EDTA; (*S*)NBD, ((*S*)-2-(4-nitrobenzyl)-DOTA).

(6) Reardan, D. T.; Meares, C. F.; Goodwin, D. A.; McTigue, M.; David, G. S.; Stone, M. R.; Leung, J. P.; Bartholomew, R. M.; Frincke, J. M. *Nature* **1985**, *316*, 265−268.
(7) Goodwin, D. A.; Meares, C. F.; McCall, M. J.; McTigue, M.; Chaovapong, W. *J. Nucl. Med.* **1988**, *29*, 226−234.
(8) Goodwin, D. A.; Meares, C. F.; Watanabe, N.; McTigue, M.; Chaovapong, W.; Ransone, C. M.; Renn, O.; Greiner, D. P.; Kukis, D. L.; Kronenberger, S. I. *Cancer Res.* **1994**, *54*, 5937−5946.
(9) Loncin, M. F.; Desreux, J. F.; Merciny, E. *Inorg. Chem.* **1986**, *25*, 2646−2648.
(10) Moi, M. K.; Meares, C. F.; DeNardo, S. J. *J. Am. Chem. Soc.* **1988**, *110*, 6266−6267.
(11) Izatt, R. M.; Pawlak, K.; Bradshaw, J. S.; Bruening, R. L. *Chem. Rev.* **1995**, *95*, 2529−2586.

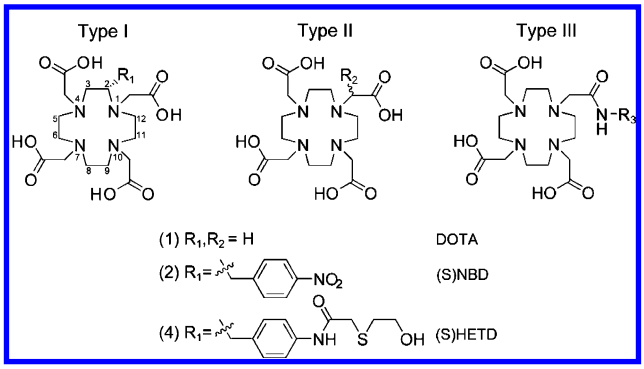

Figure 1. DOTA analogues used as probes,[15] showing sites of attachment to other molecules (R_1, R_2, R_3). Type I analogues bind to antibody 2D12.5; the S enantiomer binds more tightly than the R enantiomer.

covalently linking DOTA complexes to other molecules such as proteins;[15] other modifications have been reported to enhance water exchange properties.[16] Attachment of side chains proceeds via substitution at one of the following sites: (I) an ethylenic carbon of the macrocycle, (II) a methylene carbon bridging one of the macrocyclic amine atoms to a carboxylate carbon atom, or (III) replacement of a noncoordinating carboxylate oxygen (Figure 1). The first two methods of substitution produce an asymmetric carbon center and do not affect the overall charge of the molecule. The enantiomeric purity of an asymmetric center of the first type has been demonstrated to be stable to synthetic modifications.[17]

Recently we discovered that 2D12.5 binds the DOTA chelates of *all* the lanthanides with similar affinities,[18] potentially making it a molecular docking station for medical imaging and therapy and other biotechnological applications. Such scope is unusual among anti-chelate antibodies, which bind chelates of one or perhaps two metals with high affinity.[6,19,20] We have determined the crystal structures of antibody 2D12.5 bound to an yttrium-DOTA analogue and separately to a gadolinium-DOTA analogue, to better understand how this occurs.[21]

Materials and Methods

Materials. Antibody 2D12.5 purified from hybridoma cell culture was a gift from Dr. David Goodwin, Palo Alto Veterans Administration Hospital, Palo Alto, CA. Agarose immobilized papain, Ultralink immobilized protein G, and Supersignal Pico chemiluminescent ELISA substrate were obtained from Pierce, Rockford, IL. Endo F2 was purchased from Prozyme, San Leandro, CA. Goat anti-mouse λ-horseradish peroxidase conjugate was purchased from Southern Biotechnology Associates, Inc., Birmingham, AL. Lumitrac 600 microplates were supplied by Greiner Bio-One, Longwood, FL. Hexahydrate chloride salts of yttrium and gadolinium were purchased from Sigma Aldrich (St. Louis, MO) and were obtained in their highest available purity. Ultrafree centrifugal protein concentrators (10 000 MWCO) were obtained from Millipore, Bedford, MA. Analytical reversed phase HPLC was performed on an Altima 4.6 × 250 mm C18 column (Alltech Associates, Inc., Deerfield, IL). A Superdex 200 HR 10/30 gel filtration column was purchased from Amersham Biosciences, Piscataway, NJ. Chemiluminescence was detected with a Lumistar luminometer (BMG LabTechnologies, Durham, NC). Pure water (18 MΩ cm) was used throughout.

Sequencing of Variable Domains of 2D12.5. Poly-adenylated mRNA was purified from 2D12.5 hybridoma cells by standard techniques. cDNA was obtained using Novagen's Mouse Ig-Primer kit, which incorporates degenerate 3′ constant domain primers specific to mouse IgG genes. Double stranded DNA was obtained from cDNA using degenerate 5′ and 3′ primers provided in the Mouse Ig-Primer kit. The heavy and light chain variable genes, each with an unpaired 3′ terminal A, were cloned separately into a pT7Blue T-vector and sequenced. The constant domain sequence of the light chain was later obtained from poly-A mRNA using degenerate primers, while limited attempts to obtain the sequence of the C_{H1} domain were unsuccessful. Analysis of the Kabat database led to the selection of a consensus sequence for the C_{H1} domain that was used to solve the crystal structure; the electron density supports the Kabat-derived consensus sequence. The sequences of the light and heavy chain variable (V_L and V_H) domains are provided in Supporting Information.

Preparation of Chelates. (*S*)NBD, its enantiomer (*R*)NBD, and (*S*)-BAD were prepared as described previously.[10,17,22] (*S*)BAD was converted to (*S*)HETD by alkylation of 2-mercaptoethanol as follows: (*S*)BAD (1.8 μmol) dissolved in 50 μL of 0.1 M tetramethylammonium phosphate, pH 8.8, was reacted with 1.5 equiv (1.9 μL) of 2-mercaptoethanol at 37 °C for 20 min. The solution was maintained at pH 9 with triethylamine. The product was purified by reverse-phase HPLC using the following gradient: (solvent A) water with 0.1% TFA; (solvent B) CH_3CN with 0.085% TFA, 0−5 min, 5% B, 5−42 min, 5−60% linear solvent B, 1 mL/min. Purity was confirmed by analytical HPLC and ESI-MS: *m*/*z* (MH^+) 628. Metal ions were complexed with the chelates, and relative antibody binding affinities were measured by competitive ELISA.[18]

Antibody Deglycosylation. Observation of 2D12.5 Fab heterogeneity by SDS-PAGE and identification of an N-linked glycosylation sequence at position 85 (Kabat numbering[23]) of the heavy chain led us to deglycosylate the antibody with Endo F2. Approximately 100 mg of antibody 2D12.5 purified from hybridoma cell culture (~8.4 mg/mL) was dialyzed into 50 mM NaOAc, pH 4.5. Endo F2 was added (1.6 μU per μg of total protein), and the solution was placed in a 10 000 NMWL dialysis cassette and allowed to incubate for several days at 37 °C. A large amount of protein was treated with a relatively small amount of Endo F2 (recommended 50 μU per μg protein); therefore, the outer 50 mM NaOAc, pH 4.5 buffer was exchanged daily to minimize enzyme inhibition by cleaved glycans. The enzymatic reaction was monitored by SDS-PAGE.

2D12.5 Fab Preparation. Deglycosylated antibody 2D12.5 (approximately 100 mg) was dialyzed into a neutral buffer (20 mM sodium phosphate, 10 mM EDTA, pH 7). The protein solution was diluted by half into the same buffer containing cysteine (20 mM) immediately prior to the addition of 10 mL of papain gel (immobilized on cross-linked, 6% beaded agarose) pre-equilibrated in the same buffer. The mixture was agitated for 16 h at 37 °C, and the digestion progress was monitored using a Superdex 200 HR 10/30 gel filtration column

(12) Mikola, H.; Takalo, H.; Hemmila, I. *Bioconjugate Chem.* **1995**, *6*, 235−241.
(13) Caravan, P.; Ellison, J. J.; McMurry, T. J.; Lauffer, R. B. *Chem. Rev.* **1999**, *99*, 2293−2352.
(14) Parker, D.; Dickins, R. S.; Puschmann, H.; Crossland, C.; Howard, J. A. *Chem. Rev.* **2002**, *102*, 1977−2010.
(15) Liu, S.; Edwards, D. S. *Bioconjugate Chem.* **2001**, *12*, 7−34.
(16) Zhang, S.; Wu, K.; Sherry, A. D. *J. Am. Chem. Soc.* **2002**, *124*, 4226−4227.
(17) Renn, O.; Meares, C. F. *Bioconjugate Chem.* **1992**, *3*, 563−569.
(18) Corneillie, T. M.; Whetstone, P. A.; Fisher, A. J.; Meares, C. F. *J. Am. Chem. Soc.* **2003**, *125*, 3436−3437.
(19) Bosslet, K.; Steinstraesser, A.; Hermentin, P.; Kuhlmann, L.; Bruynck, A.; Magerstaedt, M.; Seemann, G.; Schwarz, A.; Sedlacek, H. H. *Br. J. Cancer* **1991**, *63*, 681−686.
(20) Blake, D. A.; Chakrabarti, P.; Khosraviani, M.; Hatcher, F. M.; Westhoff, C. M.; Goebel, P.; Wylie, D. E.; Blake, R. C., II. *J. Biol. Chem.* **1996**, *271*, 27677−27685.
(21) The coordinates and structure factors for each crystal structure have been deposited with the RCSB Protein Data Bank as PDB ID's 1NC2 (antibody 2D12.5-Y-(*S*)HETD) and 1NC4 (antibody 2D12.5-Gd-(*S*)NBD).
(22) Meares, C. F.; McCall, M. J.; Reardan, D. T.; Goodwin, D. A.; Diamanti, C. I.; McTigue, M. *Anal. Biochem.* **1984**, *142*, 68−78.
(23) By convention, antibody sequence positions are generally assigned using the Kabat numbering scheme, which puts the residues in the binding site into a common frame of reference (see http://www.rubic.rdg.ac.uk/abs/). Comparison between the actual sequence positions and Kabat positions is given in the Supporting Information.

equilibrated in CAPS buffer. The immobilized papain was removed by centrifugation and filtration, and the resulting protein solution was concentrated by centrifugation using an Ultrafree-10 protein concentrator. Fab and contaminating Fc fragments of the same relative size were separated from undigested antibody and small proteolytic fragments by gel filtration. CAPS buffer (pH 10) was used because Fab fragments were found to have low solubility at neutral pH and concentrations greater than 1 mg/mL.

Two methods were evaluated to separate Fab from comparably sized Fc fragments. Protein A, which is known to have a low affinity for mouse IgG1 Fc,[24] did not sufficiently remove the contaminating fragments. The Fab fragments were successfully purified by an alternate strategy using immobilized protein G, which has a weak affinity for the C_{H1} (Fab) domain of mouse IgG1 antibodies.[25] The purified Fab was dialyzed extensively into CAPS buffer and concentrated to 9.6 mg/mL. A noncompetitive ELISA was used to confirm the metal complex binding activity of the purified Fab solution relative to undigested antibody.

Fab-Metal Complex Crystallization. Yttrium-(*S*)HETD, a hapten having a side chain similar to the original antigen, was used in the crystallization. The protein−hapten complex was prepared by incubating 1.8 equiv of Y-(*S*)HETD with the purified Fab (9.7 mg/mL) for several minutes. Final concentrations of protein and metal complex in a typical sample used for crystallization were 190 and 340 μM, respectively. This solution was screened for crystallization conditions by hanging-drop vapor diffusion. A typical drop contained 4 μL of a 1:1 mixture of protein−metal complex solution and crystallization solution (100 mM HEPES pH 7.5, 18−20% PEG 8000). Crystals appeared within 2 days at 290 K as thin plates with the approximate dimensions 0.75 mm × 0.25 mm × 0.05 mm. Crystals were transferred into a cryoprotectant solution (100 mM HEPES, 22% PEG 8000, 75 mM NaCl and 20% ethylene glycol) and allowed to equilibrate overnight before cryocooling under an N_2 gas stream at 100 K. After determining the conditions for crystallizing the Y-(*S*)HETD bound 2D12.5 Fab, we incubated the Gd^{3+} complex of (*S*)NBD (an analogous chelate with a shorter side chain, Figure 1) with the purified 2D12.5 Fab and crystallized it using the same methods described for the Y-(*S*)HETD hapten. Protein crystals did not form in the absence of either metal complex.

Data Collection and Phase Determination. High-resolution datasets were collected on beam line 9-2 at the Stanford Synchrotron Radiation Laboratory (SSRL). Datasets were processed using DENZO and SCALEPACK,[26] and statistics are listed in Table 1. The space group for 2D12.5 Fab bound to Y-(*S*)HETD was $P2_12_12_1$ with cell parameters of $a = 67.34$ Å, $b = 81.30$ Å, $c = 160.92$ Å. The Matthews coefficient was calculated to be 2.33 Å^3/Da assuming two Fab molecules per asymmetric unit (46.8% solvent). A highly homologous mouse IgG1-λ (PDB ID 1GIG) was used to solve the initial phases by molecular replacement with the program AMoRe.[27,28] The data used for molecular replacement were obtained from a crystal of 2D12.5 bound to Y-(*S*)-HETD. The 1GIG structure was reduced to a polyalanine model, and regions lacking 2D12.5 sequence homology, such as CDR3 of the heavy chain, were removed to minimize bias. A number of rotation function peaks were found that were used to search for the translation function. The final translation function search found two polyalanine Fab fragments with no overlaps resulting in an *R*-factor and correlation coefficient of 51.7 and 25.0%, respectively (next highest peaks clustered ∼53.5 and ∼17.5%, respectively).

The elbow angles between the variable and constant domains of crystallized Fab molecules are known to vary, since the interdomain linkers are a source of flexibility. Therefore, interdomain linkers connecting the variable and constant regions were removed to enable the treatment of the constant and variable domains as separate entities for rigid body refinement. To solve the phases, the four domains of each polyalanine Fab molecule (V_L, C_L, V_H, C_{H1}) were treated as separate units (a total of eight domains in the unit cell) and were rigid-body refined to decrease the *R*-factor to 44.4% for data to 4 Å resolution.

Table 1. Data Collection and Refinement Statistics

	data collection	
	Y-(*S*)HETD	Gd-(*S*)NBD
wavelength (Å)	0.98 (SSRL 9-2)	0.98 (SSRL 9-2)
resolution range (Å)[a]	30−2.10 (2.18−2.10)	50−2.25 (2.33−2.25)
space group	$P2_12_12_1$	$P2_12_12_1$
unit cell parameters (Å)	$a = 67.34$, $b = 81.30$, $c = 160.92$	$a = 67.57$, $b = 82.24$, $c = 160.93$
no. of reflections	127 387 (11 654)	126 214 (10 640)
no. unique	50 276 (4899)	39 939 (3602)
completeness (%)	95.9 (95.0)	91.0 (83.4)
R_{merge}[b]	0.088 (0.299)	0.089 (0.257)

	refinement statistics	
	Y-(S)HETD	Gd-(S)NBD
resolution (Å)	29.20−2.10	29.39−2.25
no. of reflections ($F \geq 0$)	50 276	39 698
R-factor[c]	0.209	0.208
R_{free}	0.247	0.248
rmsd bond lengths (Å)	0.013	0.013
rmsd bond angles (deg)	1.8	1.8
Ramachandran statistics: most favored (%)	90.4	89.1
additional allowed (%)	9.0	10.3
generously allowed (%)	0.4	0.3
disallowed (%)	0.3	0.3
asymmetric unit content:		
nonhydrogen protein atoms	6519	6518
solvent atoms	362	332
heteroatoms	104	94

[a] Values in parentheses refer to the highest resolution shell. [b] $R_{merge} = [\sum_h\sum_i|I_h - I_{hi}|/\sum_h\sum_i I_{hi}]$, where I_h is the mean of I_{hi} observations of reflection *h*. Numbers in parentheses represent highest resolution shell. [c] *R*-factor and $R_{free} = \sum||F_{obs}| - |F_{calc}||/\sum|F_{obs}| \times 100$ for 95% of recorded data (*R*-factor) or 5% of data (R_{free}). Numbers in parentheses represent highest resolution shell.

Model Building and Refinement of Y-(S)HETD Bound to 2D12.5 Fab. After solving the initial phases, we used the molecular graphics program ***O*** for model building.[29] Energy minimization and individual *B*-factor refinement were completed with the crystallography program CNS restraining noncrystallographic symmetry.[30] The electron density for Y^{3+} was visible in the initial model, but the chelate was observable only as a diffuse cloud of density because CDR3 of the heavy chain and side chains were still missing from the model. After several reiterative steps of incorporating side chains into the model, the density for CDR3 of the heavy chain became clearly outlined in the $2F_o - F_c$ electron density map contoured at 1 σ. At this stage, the CDR3 loops were built using ***O***, and further modeling and refinement of the two Fab molecules was completed independently without noncrystallographic symmetry restraints. After including the CDR3 loop of the heavy chain in the model, the density for the Y-(*S*)HETD chelate became more clearly defined. The variable and constant domain linkers were added after CDR3 of the heavy chain was built, and solvent exposed loops and C-terminal domains were added in the later stages of refinement. Although the interchain disulfides of the Fab molecules

(24) Akerstrom, B.; Brodin, T.; Reis, K.; Bjorck, L. *J. Immunol.* **1985**, *135*, 2589−2592.
(25) Derrick, J. P.; Wigley, D. B. *Nature* **1992**, *359*, 752−754.
(26) Otwinowski, Z.; Minor, W. *Methods Enzymol.* **1997**, *276*, 307−326.
(27) Bizebard, T.; Daniels, R.; Kahn, R.; Golinelli-Pimpaneau, B.; Skehel, J. J.; Knossow, M. *Acta Crystallogr., Sect. D* **1994**, *D50*, 768−777.
(28) Navaza, J. *Acta Crystallogr.* **1994**, *A50*, 157−163.
(29) Jones, T. A.; Zou, J.-Y.; Cowan, S. W.; Kjeldgaard, M. *Acta Crystallogr., Sect. A* **1991**, *47*, 110−119.
(30) Brunger, A. T.; Adams, P. D.; Clore, G. M.; DeLano, W. L.; Gros, P.; Grosse-Kunstleve, R. W.; Jiang, J.-S.; Kuszewski, J.; Nilges, M.; Pannu, N. S.; Read, R. J.; Rice, L. M.; Simonson, T.; Warren, G. L. *Acta Crystallogr., Sect. D* **1998**, *54*, 905−921.

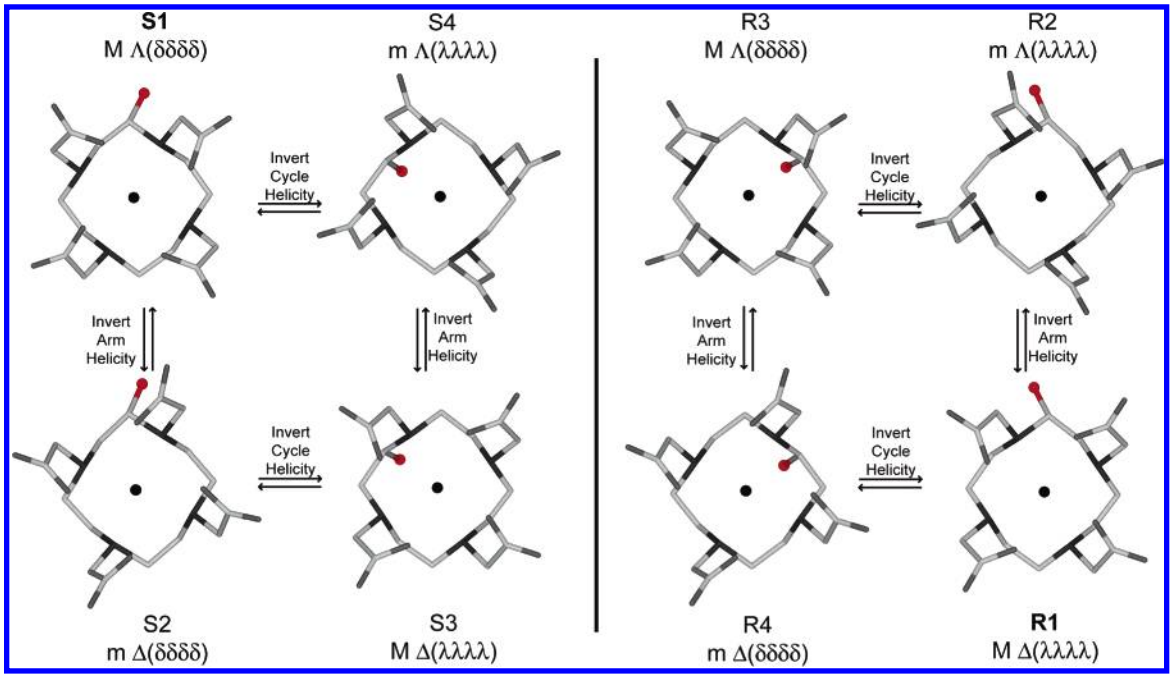

Figure 2. Stereoisomers of Type I DOTA analogues. The backbone substituent is colored red; the macrocycle is depicted behind the carboxymethyl arms. S and R represent the stereochemistry at the backbone carbon where the side chain is attached. If the substituent is hydrogen, a total of four isomers are possible in solution (S1 = R3, S2 = R4, S3 = R1, S4 = R2), and S1−S3 and S2−S4 are enantiomeric pairs. For hypothetical racemic Type I DOTA analogues such as NBD and HETD, the number of possible isomers is doubled (S1 ≠ R3, S2 ≠ R4, S3 ≠ R1, S4 ≠ R2 and S1−R1, S2−R2, S3−R3, and S4−R4 are enantiomeric pairs). For Y-(*S*)HETD and Gd-(*S*)NBD, only the S1 (**M** Λ(*δδδδ*)) isomer is significantly present in solution. For these complexes with an R backbone substituent, the dominant isomer in solution is R1.

were known to be intact by SDS-PAGE, the interchain disulfide electron density was only visible in one of the Y-(*S*)HETD bound Fab molecules as the C-terminus of the other molecule was disordered. Endo F2 processing of N-linked glycans leaves a single *N*-acetyl-D-glucosamine residue that is visibly attached to N85 of the heavy chain of the Fab molecules in the final model. Also, the genetically coded N-terminal glutamine of the heavy chain is visible as the cyclic pyroglutamate, a common posttranslational modification, in one of the molecules.

Model Building and Refinement of Gd-(*S*)NBD Bound to 2D12.5 Fab. The structure of Gd-(*S*)NBD bound 2D12.5 was expected to be similar to that solved for Y-(*S*)HETD. Therefore, a mostly refined model of the protein taken from the 2D12.5−Y-(*S*)HETD structure was used to perform a rigid body fit of the Gd-(*S*)NBD data using a high-resolution cutoff of 5 Å. The Gd-(*S*)NBD bound 2D12.5 structure was then refined separately from the Y-(*S*)HETD bound Fab data. The interchain disulfides were not visible in either of the structures in the unit cell.

Model Building of Y-DOTA and Gd-DOTA and Inclusion in Refinement. Crystal structures of Y-DOTA and Gd-DOTA were available from the Cambridge Crystallographic Data Center.[31−33] The electron density for each metal chelate bound to 2D12.5 was examined to determine the appropriate conformational isomer to use (Figure 2). The acetate arms of the Y-DOTA coordinates (Cambridge ID's LATKOG and LATKOG01) exhibited helicity (Δ(*λλλλ*)) opposite to that observed in the 2D12.5 crystal structure (Λ(*δδδδ*)), while the coordinates for both helicities were available for the Gd-DOTA structures (Cambridge ID's JOPJIH and JOPJIH01). Therefore, the mirror image of the Cambridge coordinates for Y-DOTA were used, and the appropriate Λ(*δδδδ*)-isomer coordinates were used for the Gd-DOTA structure.

The Y-DOTA and Gd-DOTA chelates were included in the refinements of the crystal structure of 2D12.5 after CDR3 of the heavy chain had been added to the model. It was at this stage that the density for each DOTA chelate became articulated. The M-DOTA chelates were first placed into the structure without the addition of the 2-(4-(2-(2-hydroxyethylthio)-acetamido)-benzyl)- or 2-(4-nitrobenzyl)- side chains because the electron density for the side chains was not obvious at this point. The Hetero-compound Information Center database (HIC-UP)[34] was used to prepare parameter and topology files for the Y-DOTA and Gd-DOTA structures that were compatible with CNS. Real-space refinement of the Y-DOTA and Gd-DOTA chelate conformations was performed with X-LIGAND (Accelrys)[35] because the electron density for the DOTA chelates differed slightly from the initial models.

When most of the protein model had been completed and waters had been added to each model, the 2-(4-(2-(2-hydroxyethylthio)-acetamido)-benzyl)- and 2-(4-nitrobenzyl)- side chains were added to the Y-DOTA and Gd-DOTA coordinates, respectively, which had been refined in X-Ligand and CNS. These structures were modified with the Builder module of the program Insight II (Accelrys) to include the appropriate side chain. While building the model, it became clear that the isomer that placed the side chain in an equatorial orientation was energetically most favorable. The equatorial position and chirality of (*S*)HETD further confers the Λ-helicity to the acetate arms. As expected, a minimized model of (*R*)HETD showed that the Δ-helicity of the acetate arms is most favored for an equatorial placement of the side chain. Atom potentials were defined with the extensible systematic force field (esff), and a steepest descent algorithm in Discover 3 (Accelrys) was used to obtain minimized side chain conformations while leaving the DOTA moiety of Y-(*S*)HETD and Gd-(*S*)NBD structures unchanged. Parameter and topology files were obtained from the HIC-UP server, and the models were then included in the crystal structure model refinements with CNS. Available conformations for the benzyl portion of the side chain seemed limited during the refinement. This

(31) Chang, C. A.; Francesconi, L. C.; Malley, M. F.; Kumar, K.; Gougoutas, J. Z.; Tweedle, M. F.; Lee, D. W.; Wilson, L. J. *Inorg. Chem.* **1993**, *32*, 3501−3508.
(32) Parker, D.; Pulukkody, K.; Smith, F. C.; Batsanov, A.; Howard, J. A. K. *J. Chem. Soc., Dalton Trans.* **1994**, 689−693.
(33) Dubost, J. P.; Leger, J. M.; Langlois, M. H.; Meyer, D.; Schaefer, M. *C. R. 'Acad. Sci., Ser. II: Mec., Phys., Chim., Sci. Terre Univers* **1991**, *312*, 349−354.
(34) Kleywegt, G. J.; Jones, T. A. *Acta Crystallogr., Sect. D* **1998**, *54*, 1119−1131.
(35) Oldfield, T. J. *Acta Crystallogr., Sect. D* **2001**, *57*, 696−705.

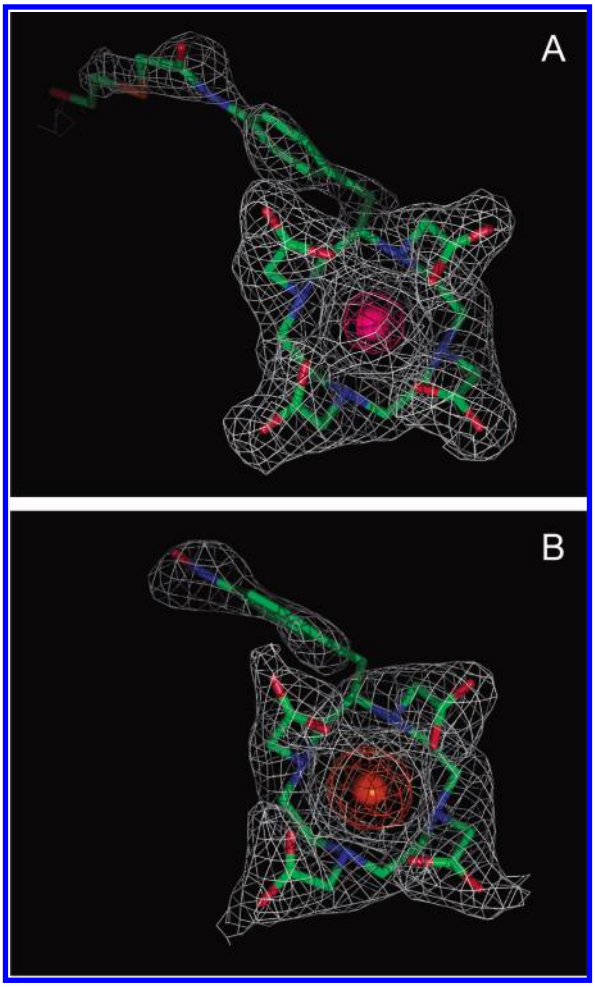

Figure 3. Fits of Y-(*S*)HETD (A) and Gd-(*S*)NBD (B) to the $2F_o - F_c$ electron density maps contoured at 1 σ. A second contour of the $2F_o - F_c$ electron density map has been rendered at 10 σ for Y^{3+} (colored magenta) and Gd^{3+} (colored orange) and clearly shows the considerably higher electron number for Gd^{3+}. The electron density of the DOTA ligand surrounding the metal ion is clearly resolved for the Y-(*S*)HETD, while the density for the carboxylates of the DOTA ligand in the Gd-(*S*)NBD structure is slightly more ambiguous, presumably due to the increased number of electrons for the Gd^{3+} ions and slightly lower resolution. Only one of each metal complex (two nonsymmetry related hapten-bound Fab molecules are present in each unit cell) is shown from each structure because the others are similar. Figures were prepared with PyMol.[36]

observation was later supported by the $2F_o - F_c$ electron density at 1 σ, which clearly shows the orientation of the benzyl portion of the side chain while the density for more peripheral atoms of the side chain is less clear for each of the models.

Overall Structures. The overall atomic resolution for each of the data sets is 2.1 and 2.25 Å, for 2D12.5 mAb bound to Y-(*S*)HETD and Gd-(*S*)NBD, respectively (Table 1). Each asymmetric unit contains two metal complex-bound Fab molecules, so the two structures yield information for four Fab molecules.

The $2F_o - F_c$ electron density (1 σ) for the metal ions is clearly defined in all cases. The DOTA ligands surrounding the metal ions are clearly resolved in the Y-(*S*)HETD structure, while the density for each of the DOTA ligands in the Gd-(*S*)NBD structure is slightly more ambiguous, presumably due to the increased number of electrons for the Gd^{3+} ions (61e for Gd^{3+}, 36e for Y^{3+}) and slightly lower resolution. In all cases, the orientations of the coordinating acetate arms of the DOTA ligands are clear (Figure 3), and the density for the surrounding protein residues is well-defined. The side chains of the chelate molecules are resolved up to the benzyl group for each Fab molecule; however, the lack of binding interactions between the side chain and the protein and the inherent flexibility within the 2-(4-(2-(2-hydroxyethylthio)-acetamido)-benzyl side chain apparently lead to its disorder in the final structure. The conformation observed for one of two (*S*)HETD side chains present in the unit cell is influenced by a crystal packing interaction with a symmetry related Fab molecule. In addition, there are at least four ordered water molecules in each binding cavity bridging the chelate and the protein.

For the mAb 2D12.5 structures bound to Y-(*S*)HETD and Gd-(*S*)-NBD, a total of 90.4 and 89.1% of the residues fall within the most favored region of a Ramachandran plot. Only the S93 residue of each light chain exhibits a disallowed Phi/Psi angle as determined by the program PROCHECK.[37] The observed Phi/Psi values in each Fab molecule (approximately 60°/−40°) indicate that S93(L) is the $i + 1$ residue in a gamma turn, similar to the corresponding values for S93-(L) in the Fab molecule 1GIG which was used for molecular replacement.

Results and Discussion

Observed Isomers. When the DOTA macrocycle wraps around a metal ion, it assumes a helical twist. A bulky substituent on a backbone carbon of the macrocycle can determine the handedness of the helix. As illustrated in Figure 2, there are eight possible isomers for backbone-substituted DOTA chelates. Unsubstituted Y-DOTA and Gd-DOTA are known to exist in solution as primarily the **M** isomers.[38,39] Fits to the electron density illustrated in Figure 3 indicate that only the $\Lambda(\delta\delta\delta\delta)$ enantiomers of Y-(*S*)HETD and Gd-(*S*)NBD are observed in the metal complex-bound crystal structures of mAb 2D12.5. The energetically favorable $\Lambda(\delta\delta\delta\delta)$ helicities observed for the side chain DOTA complexes Y-(*S*)HETD and Gd-(*S*)-NBD are predicted by theoretical models and are a consequence of the single asymmetric carbon where the side chain is attached to the macrocycle. The equatorial conformation observed in the crystal structure models is energetically favored over an axial position of the side chain, which produces steric clashes between the macrocycle and chelate side chain.

The (*S*)HETD and (*S*)NBD side chains do not appear to interact with the protein in either structure (Figure 4). Y-DOTA and Gd-DOTA exhibit C_4 symmetry; a repeated 90° rotation of the molecule around the central axis yields the same molecule. Incorporation of a (*S*)HETD or (*S*)NBD side chain destroys the C_4 symmetry, but because the (*S*)HETD and (*S*)NBD side chains do not interact with the protein, the rotational symmetry of the metal-DOTA moiety is still important. In fact, two orientations of the side chain are observed in each of the crystal structures. For each complex, the orientation that is best resolved in the electron density maps is represented in the final structures in Figure 4. The metal-DOTA moiety lies at an angle in the binding cavity. The other possible orientations are prevented because of potential steric clashes between the (*S*)HETD and (*S*)NBD side chains with the protein. A 90° rotation of the DOTA moiety represents the difference between the two possible (*S*)HETD and (*S*)NBD side chain orientations. The other two orientations would place the side chain too close to aromatic side chain residues Trp52 (CDR2(H)), Tyr32 (CDR1(L)), or Trp91 (CDR3-(L)). An unsubstituted metal-DOTA complex would not have

(36) DeLano, W. L. *The PyMOL Molecular Graphics System*; DeLano Scientific: San Carlos, CA, 2002 (http://www.pymol.org).
(37) Laskowski, R. A.; MacArthur, M. W.; Moss, D. S.; Thornton, J. M. *J. Appl. Crystallogr.* **1993**, *26*, 283−291.
(38) Aime, S.; Botta, M.; Fasano, M.; Marques, M. P.; Geraldes, C. F.; Pubanz, D.; Merbach, A. E. *Inorg. Chem.* **1997**, *36*, 2059−2068.
(39) Cosentino, U.; Villa, A.; Pitea, D.; Moro, G.; Barone, V.; Maiocchi, A. *J. Am. Chem. Soc.* **2002**, *124*, 4901−4909.

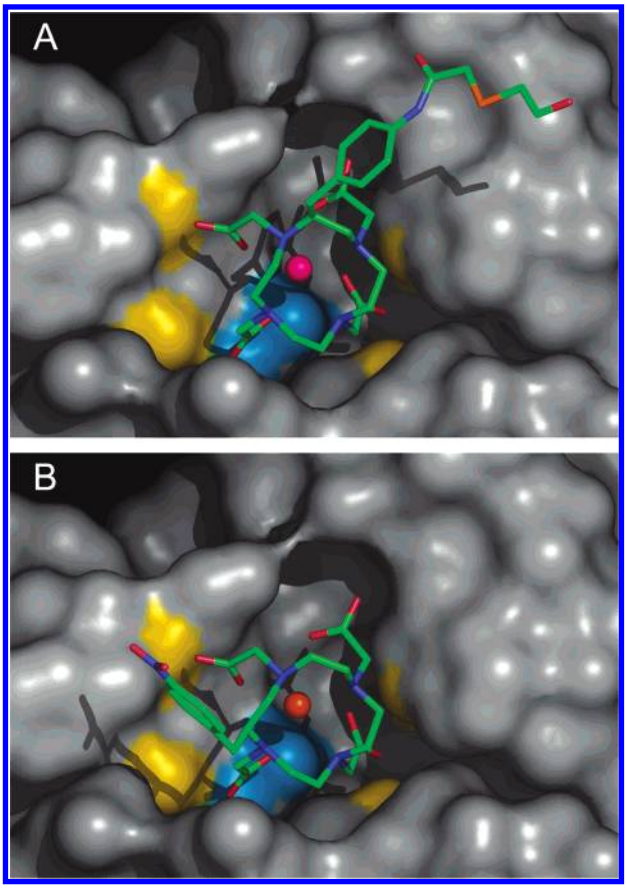

Figure 4. Comparison of the structures of (A) antibody 2D12.5 bound to Y−(*S*)HETD and (B) antibody 2D12.5 bound to Gd-(*S*)NBD. Each metal chelate is rendered as a stick model, with the metal as a sphere. The antibody is rendered as a surface, showing the binding cleft. At the bottom of the binding cleft in blue is Arg95(H), whose side chain forms a stabilizing salt bridge with a DOTA carboxylate; in yellow (clockwise from top right) are the side chain nitrogen atoms of Trp52(H), Trp96(L), and Asn100A(H), and the main chain amide nitrogen of Tyr98(H), which form hydrogen bonds to DOTA carboxylates. In each case, the antibody structure is the same within experimental error, but the (*S*)HETD side chain is rotated 90° relative to the (*S*)NBD side chain (see text).

the side chain interference presented by (*S*)HETD and (*S*)NBD and so could bind in any of four equivalent orientations.

Binding Interactions. Analysis of the binding cavity indicates that there are no significant perturbations of the protein backbone or protein side chains between the structural models of 2D12.5 bound to Y-(*S*)HETD and Gd-(*S*)NBD. Any movement of the protein between the structures is within the rmsd values for the protein structure. Therefore we focus on the structural model of 2D12.5 bound to Y-(*S*)HETD below; similar observations hold for 2D12.5 bound to Gd-(*S*)NBD.

Residues at the top of the CDR3(H) loops are unique to a particular antibody and normally play an important role in shaping the binding cavity and determining antigen binding;[40,41] antibody 2D12.5 is no exception. The top of the CDR3(H) loop of 2D12.5 is comprised of a *cis*-proline residue sandwiched between two tyrosine side chains (Figure 5). This unusual feature is associated with hydrogen bonds involving Gly96(H) and Tyr98(H).

The specific binding interaction between antibody 2D12.5 and its metal complex haptens has an interesting flexibility that

(40) Chothia, C.; Lesk, A. M. *J. Mol. Biol.* **1987**, *196*, 901−917.
(41) Xu, J. L.; Davis, M. M. *Immunity* **2000**, *13*, 37−45.

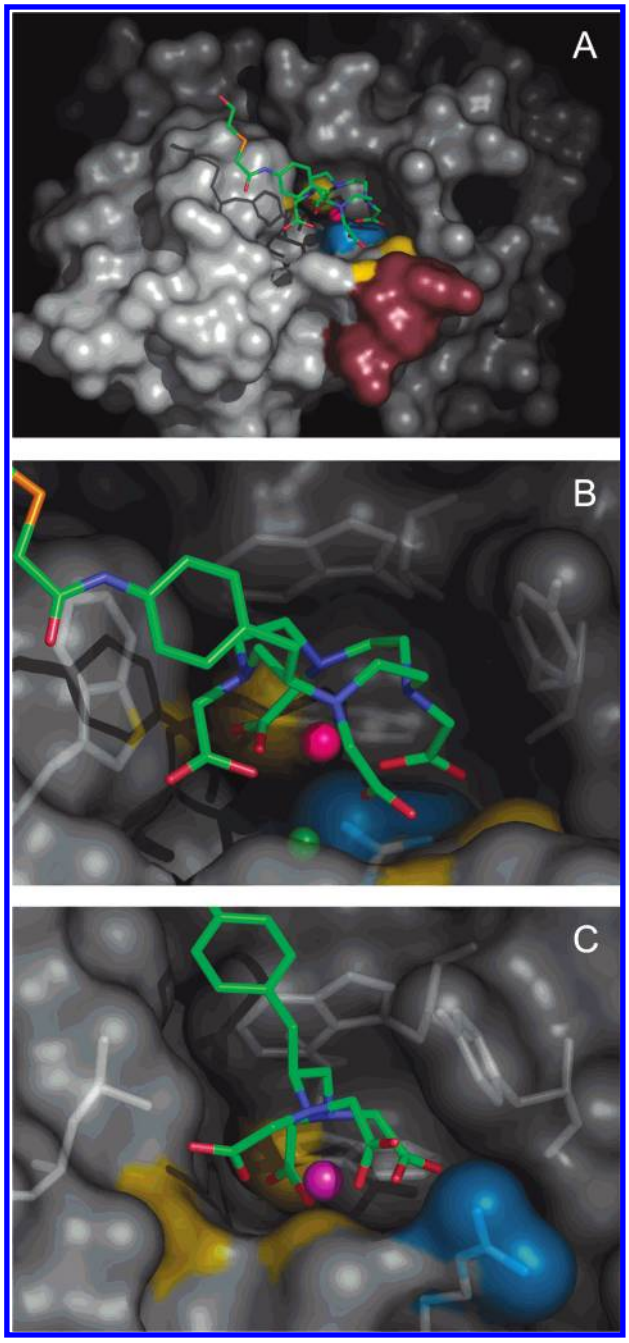

Figure 5. (A) View of the surface of the 2D12.5−Y-(*S*)HETD complex, with Y-(*S*)HETD depicted as a stick model and the antibody rendered to show the binding cleft. At the top of the binding cleft in reddish brown is the distinctive Tyr98/Pro99/Tyr100 stacked arrangement that is part of the heavy-chain CDR3 region of 2D12.5. Note that no van der Waals contacts with the HETD backbone substituent are evident. (B) Closer view of the 2D12.5−Y-(*S*)HETD binding site, showing the annular arrangement of the aromatic side chains that surround the DOTA. The yttrium is rendered in magenta, and the oxygen of the coordinated water molecule is green. The Gd-(*S*)NBD complex has the same features. (C) View of the indium-binding antibody CHA255−In-(S)EOTUBE structure (PDB ID 1IND) in the same orientation. There is no Tyr/Pro/Tyr stack, but there is an annular arrangement of hydrophobic side chains around the EDTA group similar to that observed in the 2D12.5−Y-(*S*)HETD and 2D12.5−Gd-(*S*)NBD crystal structures. The indium ion (purple) is directly coordinated to the His95(H) side chain (yellow). A carboxylate of EOTUBE, a side chain derivative of EDTA, interacts with Arg96(H) (blue) at the top of the binding cleft. Hydrogen bonds are formed between other EDTA carboxylates and the side chain atoms of Trp96(L) and Thr33(H) (also colored yellow).

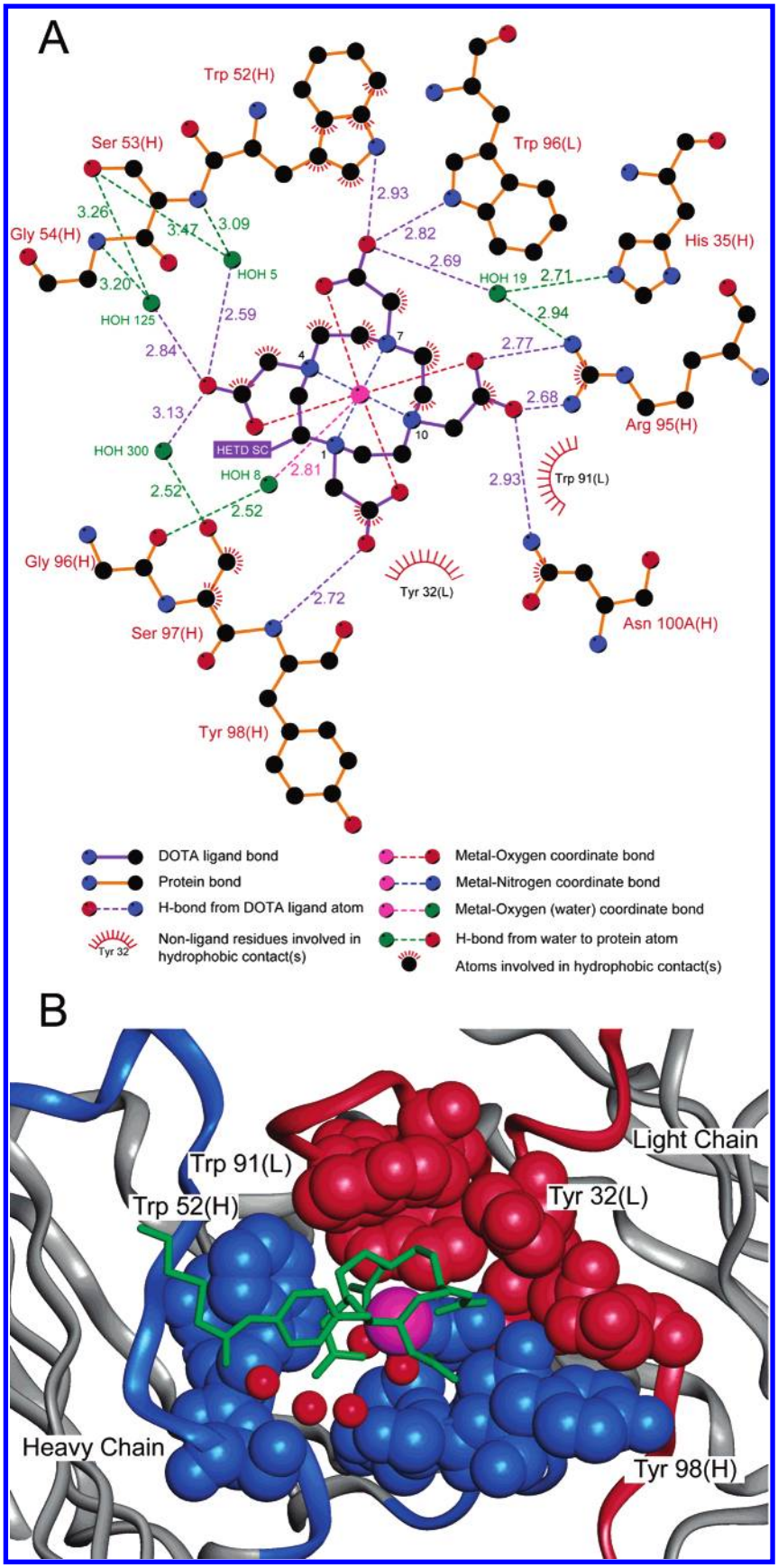

Figure 6. (A) Diagram showing the principal contacts between antibody and hapten in the 2D12.5−Y-(*S*)HETD complex, including five crystallographic water molecules. The Gd-(*S*)NBD is very similar. Figure was designed with the aid of Ligplot.[44] (B) Three-dimensional structure showing the crystallographic bridging water molecules and the protein side chains within 5 Å of the Y-(*S*)HETD. Figure was prepared with InsightII (Accelrys).

allows the substitution of any lanthanide ion into the DOTA moiety. The different metal-DOTA complexes show quantitative, but not qualitative, differences in binding affinity.[18] The structure provides several insights into this. First, there is no direct interaction between the metal and the protein. The DOTA moiety fills eight of nine available coordination sites for either Y^{3+} or Gd^{3+}. An inner sphere water molecule fills the final coordination site of the metal (Figure 5) and is observed in both the Y-(*S*)HETD and Gd-(*S*)NBD structures. This water molecule appears to be protected from the solvent, is conserved in all of the structures, and bridges the metal complex and protein by forming a hydrogen bond with the carbonyl oxygen of Gly96-(H) in CDR3(H). The metal-inner sphere water (M−O) distance ranges from 2.81 to 2.88 Å, which is longer than the approximately 2.5 Å M−O bond distance normally observed for Y-DOTA and Gd-DOTA, perhaps due to the bridging H-bond with the protein.

The binding interactions between the metal complex and the antibody include a bidentate salt bridge, five direct H-bonds, four to five water-mediated H-bonds, and numerous hydrophobic contacts (Figure 6). The DOTA moiety forms an amphipathic cylinder with the charged carboxylate groups toward the face of the chelate near the metal ion, while nonpolar methylene groups from the macrocycle and the carboxymethyl groups occupy the rear and sides of the molecule. The net charge of the metal-DOTA complex is negative (−1), and this charge is centered near the face of the coordinating carboxylates, where most of the polar interactions occur. The single most obvious attachment is the bidentate salt bridge between a DOTA carboxylate and an arginine side chain, Arg95(H), at the bottom of the binding cavity. For the 2D12.5−Y-(*S*)HETD structure shown in Figures 4A and 5B, the carboxylate attached to N10 of the macrocycle participates in this salt bridge; for 2D12.5−Gd-(*S*)NBD in Figure 4B, this role is played by the carboxylate attached to N1. An electrostatic potential map of the unliganded protein surface shows the binding cavity is highly positive. This salt bridge has ideal geometry[42,43] and therefore may contribute more to the binding affinity between the metal complex and 2D12.5 than any other single interaction.

For comparison, the crystal structure of the indium complex-binding antibody CHA255 shows a different salt bridge formed between a surface arginine and a ligand carboxylate, which is not as stabilizing since the geometry is not ideal and the salt bridge is more solvent exposed (Figure 5C). The structure of CHA255 includes the novel feature of direct coordination of the metal to a histidine side chain; there is no evidence of such direct metal−protein interaction in the case of 2D12.5. There is no sequence homology between the important CDR3(H) regions of the two antibodies; the length of CDR3(H) is only five residues for CHA255 but eleven for 2D12.5.

DOTA carboxylate oxygen atoms participate in all of the H-bonding interactions with the protein and are often multiply H-bonded (Figure 6). The Arg95(H) salt-bridge-forming DOTA carboxylate is also involved in a hydrogen bond with Asn100A-(H). The unusual CDR3(H) Tyr98/Pro99/Tyr100 sandwich positions the carbonyl oxygen of Gly96(H) to form a hydrogen bond to the metal-coordinated water molecule and the amide nitrogen of Tyr98(H) to form a hydrogen bond with a DOTA carboxylate oxygen (the N1 carboxylate in the Y-(*S*)HETD structure) that is 90° removed from the Arg95(H)-DOTA carboxylate salt bridge (the N10 carboxylate in the Y-(*S*)HETD structure). The next carboxylate (the N4 carboxylate in the Y-(*S*)HETD structure) lacks any direct interactions with the protein. Instead, this carboxylate forms H-bonds with three water molecules (conserved in three of the four structures; one has only two waters) that bridge interactions between the protein and metal complex. The final carboxylate (the N7 carboxylate in the Y−(*S*)HETD structure) forms H-bonds directly with the indole nitrogen atoms of Trp52(H) and Trp96(L) and with a bridging water molecule. Protein−metal complex interactions bridged by H-bonds formed across two water molecules constitute additional interactions between the protein and DOTA moiety of Y-(*S*)HETD and Gd-(*S*)NBD (Supporting Information) and constitute an extensive water network that is mostly conserved in all four structures.

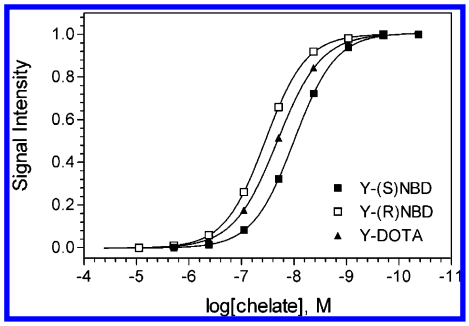

Figure 7. Binding of yttrium chelates with different stereochemistries to antibody 2D12.5, showing that the antibody binds a Type I chelate with the side chain in the R configuration approximately 1 order of magnitude less well than the S configuration (see Figure 1). Yttrium-DOTA with no side chain, which is an equal mixture of R and S, is approximately in the middle. Error bars are smaller than the data symbols. Data were generated by competitive ELISA.[18]

Tryptophan residues Trp52(H) and Trp96(L) are H-bonded to the same DOTA oxygen atom and are well positioned to serve as energy donors to a complexed lanthanide ion such as Tb^{3+}. This may be the basis of the observed 10^4-fold enhancement of Tb-DOTA luminescence upon binding to 2D12.5.[18] The π-electron clouds of nearby Trp91(L), Tyr32(L), and Trp52-(H) are oriented toward the metal (Figure 6). This abundance of aromatic residues is typical for an antibody binding cavity, and its potential for electronic excitation has been invoked in the production of blue-fluorescent antibodies.[45]

Enantiomeric Selectivity. The symmetrical nature of the metal-DOTA moiety of Y-(*S*)HETD and Gd-(*S*)NBD led us to examine the enantioselectivity of 2D12.5. Metal chelates containing polydentate ligands such as DOTA form enantiomeric complexes having opposite helicities (Figure 2). Not unexpectedly, other monoclonal antibodies developed to bind chiral metal complexes have demonstrated high selectivity for only one of the enantiomers.[6,19,20] But we discovered that antibody 2D12.5 binds Y-(R)NBD with a $\Delta\Delta G = 3.3$ kJ/mol, relative to the Y-(*S*)NBD complex (Figure 7). Interestingly, the affinity of antibody 2D12.5 for Y-(R)NBD is similar to its affinity for La-

(42) Kumar, S.; Nussinov, R. *Biophys. J.* **2002**, *83*, 1595−1612.
(43) Kumar, S.; Nussinov, R. *J. Mol. Biol.* **1999**, *293*, 1241−1255.
(44) Wallace, A. C.; Laskowski, R. A.; Thornton, J. M. *Protein Eng.* **1995**, *8*, 127−134.
(45) Simeonov, A.; Matsushita, M.; Juban, E. A.; Thompson, E. H.; Hoffman, T. Z.; Beuscher, A. E., IV; Taylor, M. J.; Wirsching, P.; Rettig, W.; McCusker, J. K.; Stevens, R. C.; Millar, D. P.; Schultz, P. G.; Lerner, R. A.; Janda, K. D. *Science* **2000**, *290*, 307−313.

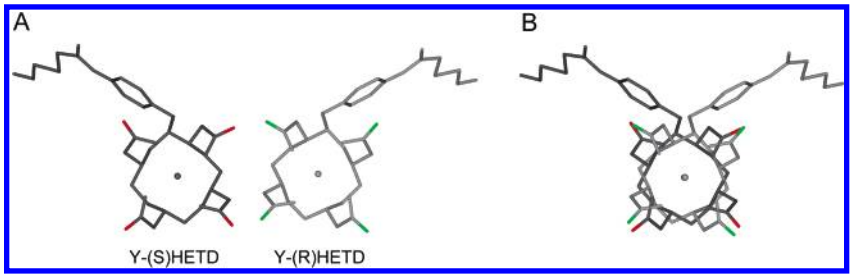

Figure 8. Noncoordinating carboxylate oxygen atoms of Y-(*S*)HETD and Y-(R)HETD are colored red and green, respectively, and are important for binding to antibody 2D12.5. Although these two molecules are enantiomers, the nature of the metal-complexed DOTA moiety allows for the two molecules and their noncoordinating carboxylate oxygen atoms to be almost superimposed.

(*S*)NBD ($\Delta\Delta G = 2.9$ kJ/mol).[18] For reference, $\Delta G° = -45.7$ kJ/mol for Y-(*S*)NBD binding to 2D12.5.

For the protein to bind both enantiomers of Y-NBD, the chiral nature of the metal complex must not significantly alter the relative position of heteroatoms or hydrophobic groups necessary for high affinity binding. In fact, the DOTA moiety of three-dimensional models of Y-(*S*)NBD and Y-(R)NBD having opposite DOTA helicities can be superimposed without much altering the relative location of carboxylate oxygens important for binding to the antibody (Figure 8). This is a result of the approximately cylindrical shape and symmetry of the metal-complexed DOTA moiety.

Consistent with these results, the binding affinity of Y-DOTA without a side chain is measured to be lower than Y-(*S*)NBD but higher than Y-(R)NBD. Y-DOTA molecules are present in solution with both $\Lambda(\delta\delta\delta\delta)$ and $\Delta(\lambda\lambda\lambda\lambda)$ helicities in equal concentration.

As with DOTA, the chirality of other metal complexes may arise simply from the wrapping of an achiral multidentate organic chelate around a metal ion. The enantiomeric purity of the resulting complex is dependent on the structure of the chelate; the complex may be a racemic mixture such as gallium-*N*,*N*′-di(2-hydroxybenzyl)ethylenediamine-*N*,*N*′-diacetic acid (Ga-HBED), or it may be practically a single stereoisomer like Y-(*S*)NBD. In one interesting example, monoclonal antibodies developed against a racemic Ga-HBED complex bind only one of the enantiomers, leaving half of the molecules unbound.[46] The chelate alone is achiral, but complexation produces a racemic mixture of Ga^{3+} complexes. Because the Ga-HBED complex is kinetically stable, it is possible to use two different antibodies to bind the isomeric metal complexes, leading to a stereochemically pure antibody−metal complex system for biological applications.

Our approach to avoid the racemic mixture of metal complexes formed between an achiral ligand and a metal is to develop a chiral chelate that favors a single enantiomer when complexed to a metal ion. The monoclonal antibody CHA255 was developed against a stereochemically pure (*S*)benzyl−EDTA complex of In^{3+}.[6] Not surprisingly, the nonpreferred enantiomer binds with an affinity that is almost 2 orders of magnitude lower than the original antigen. An unsubstituted EDTA−indium complex lacking a side chain binds more strongly than the disfavored side chain−EDTA isomer, probably because half of the metal complexes have the favored chirality. The crystal structure of the hapten-bound antibody complex clearly displays a preference for a single EDTA isomer.[47] It seems clear from these pioneering studies that the stereochemistry of the molecule (conferred by the asymmetric attachment of the side chain) determines the appropriate shape required for high affinity binding.

Table 2. Rare Earth Properties

applications	
therapy	imaging
β-particle emission	lanthanide luminescence
^{90}Y, 2.27 MeV, $T_{1/2} = 64$ h	Eu, Tb, Dy, Sm
^{153}Sm, multiple, $T_{1/2} = 47$ h	magnetic resonance imaging
^{165}Dy, 1.4 MeV, $T_{1/2} = 2.3$ h	Gd
^{166}Ho, 1.8 MeV, $T_{1/2} = 27$ h	positron emission tomography
^{169}Er, 0.35 MeV, $T_{1/2} = 9.4$ d	^{86}Y, $T_{1/2} = 14.7$ h
^{177}Lu, 0.50 MeV, $T_{1/2} = 6.7$ d	

Conclusions

This antibody−metal complex system provides generality for two reasons. First, all DOTA complexes of the rare earths, because of their chemical and physical similarities, bind with comparably high affinities to antibody 2D12.5. Because there are no direct protein−metal interactions, the binding interactions between the antibody and metal-DOTA complex are only indirectly affected by changing the metal. The second source of generality develops from the symmetrical, approximately cylindrical nature of the DOTA chelate, which places heteroatoms and hydrophobic atoms in approximately the same relative position regardless of the helicity of the Y-DOTA moiety. However, this generality apparently does not extend to metals other than yttrium and the lanthanides; while the binding constants of the latter DOTA complexes to 2D12.5 vary by less than a factor of 5, DOTA complexes of trivalent metals such as scandium or indium bind with much lower affinities (<1% of Y-DOTA).

The class of metallic elements that can bind to this antibody is rich in useful physical properties for applications in sensing, analysis, and even medical therapy. For example, the luminescence properties of terbium and europium, long excited-state lifetimes and sharp emission lines, have led to practical assays in the laboratory.[12−14] The paramagnetism of gadolinium and other lanthanides has led to contrast agents for magnetic resonance imaging.[38,39] And the nuclear emissions of yttrium, lutetium, and several of the other lanthanides have present and future uses in medical imaging and therapy.[15] Table 2 gives some examples.

(46) Zoller, M.; Schuhmacher, J.; Reed, J.; Maier-Borst, W.; Matzku, S. *J. Nucl. Med.* **1992**, *33*, 1366−1372.

(47) Love, R. A.; Villafranca, J. E.; Aust, R. M.; Nakamura, K. K.; Jue, R. A.; Major, J. G., Jr.; Radhakrishnan, R.; Butler, W. F. *Biochemistry* **1993**, *32*, 10950−10959.

Acknowledgment. This work was supported by Research Grant CA16861 to C.F.M. from the National Institutes of Health. All of the data reported were collected at SSRL, which is operated by the Department of Energy, Office of Basic Energy Sciences. The SSRL Biotechnology Program is supported by the National Institutes of Health, National Center for Research Resources, Biomedical Technology Program and by the U.S. Department of Energy, Office of Biological and Environmental Research. We thank Angelo Gunasekera for early work in isolating 2D12.5 cDNA and obtaining the variable domain sequences; Eric Lansdon, Nathan Butlin and Paul Whetstone for helpful discussions regarding the crystallography work; and Saul Datwyler, Brian Schmidt and A.J. Chmura for helpful discussions regarding the preparation and purification of Fab and synthetic chelates.

Supporting Information Available: Additional experimental and structural details and Kabat and PDB numbering systems for the Fab heavy and light chain sequences are provided in the Supporting Information (PDF). This material is available free of charge via the Internet at http://pubs.acs.org.

JA037236Y